Journal Pre-proof

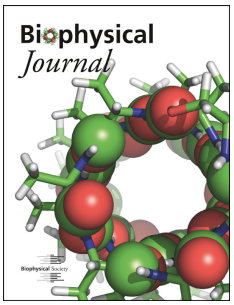

Gating kinetics and pharmacological properties of small conductance calcium-activated potassium channels

Ilsbeth G.M. van Herck, Vincent Seutin, Bo H. Bentzen, Neil V. Marrion, Andrew G. Edwards

PII: S0006-3495(23)00096-6

DOI: https://doi.org/10.1016/j.bpj.2023.02.004

Reference: BPJ 12365

To appear in: *Biophysical Journal*

Received Date: 20 July 2022

Accepted Date: 6 February 2023

Please cite this article as: van Herck IGM, Seutin V, Bentzen BH, Marrion NV, Edwards AG, Gating kinetics and pharmacological properties of small conductance calcium-activated potassium channels, *Biophysical Journal* (2023), doi: https://doi.org/10.1016/j.bpj.2023.02.004.

Gating kinetics and pharmacological properties of small conductance calcium-activated potassium channels

Ilsbeth G.M. van Herck[1,2], Vincent Seutin[3], Bo H. Bentzen[4,5], Neil V. Marrion[6], Andrew G. Edwards[1,7]

Affiliations

[1]*Computational Physiology Department, Simula Research Laboratory, Oslo, Norway*
[2]*Institute of informatics, University of Oslo, Norway*
[3]*Neurophysiology unit, GIGA Neurosciences, University of Liège, Liège, Belgium*
[4]*Acesion Pharma, Copenhagen, Denmark*
[5]*Biomedical Institute, University of Copenhagen, Copenhagen, Denmark*
[6]*School of Physiology, Pharmacology and Neuroscience, University of Bristol, Bristol, United Kingdom*
[7]*Department of Pharmacology, University of California, Davis, CA, USA*

Email of corresponding author: andy@simula.no

Abstract

Small conductance calcium-activated potassium (SK) channels are a promising treatment target in atrial fibrillation. However, the functional properties that differentiate SK inhibitors remain poorly understood. The objective of this study was to determine how two unrelated SK channel inhibitors, apamin and AP14145, impact SK channel function in excised inside-out single channel recordings. Surprisingly, both apamin and AP14145 exert much of their inhibition by inducing a class of very long-lived channel closures (apamin: $\tau_{c,vl}$=11.8±7.1 s, and AP14145: $\tau_{c,vl}$=10.3±7.2 s), which were never observed under control conditions. Both inhibitors also induced changes to the three closed and two open durations typical of normal SK channel gating. AP14145 shifted the open duration distribution to favor longer open durations, whereas apamin did not alter open state kinetics. AP14145 also prolonged the two shortest channel closed durations (AP14145**:** $\tau_{c,s}$=3.50±0.81 ms, and $\tau_{c,i}$=32.0±6.76 ms vs. control: $\tau_{c,s}$=1.59±0.19 ms, and $\tau_{c,i}$=13.5±1.17 ms), thus slowing overall gating kinetics within bursts of channel activity. In contrast, apamin accelerated intra-burst gating kinetics by shortening the two shortest closed durations ($\tau_{c,s}$=0.75±0.10 ms and $\tau_{c,i}$=5.08±0.49 ms), and inducing periods of flickery activity. Finally, AP14145 introduced a unique form of inhibition by decreasing unitary current amplitude. SK channels exhibited two clearly distinguishable amplitudes (control: A_{high}=0.76±0.03 pA**,** and A_{low}=0.54±0.03 pA). AP14145 both reduced the fraction of patches exhibiting the higher amplitude (AP14145: 4/9 patches vs. control: 16/16 patches), and reduced the mean low amplitude (0.38±0.03 pA). Here we have demonstrated that both inhibitors introduce very long channel closures, but that each also exhibits unique effects on other components of SK gating kinetics and unitary current. The combination of these effects is likely to be critical for understanding the functional differences of each inhibitor in the context of cyclical Ca^{2+}-dependent channel activation *in vivo*.

Statement of significance

Due to their prevalence in the atria, and activity-dependent activation, small conductance calcium-activated potassium (SK) channels are an attractive target for treatment of atrial fibrillation. However, the mechanisms by which the gating and activity of these channels are altered by pharmacological agents remains poorly understood. Here we apply excised single channel patch clamp to discern the impacts of two developmentally unrelated SK channel inhibitors, apamin and AP14145. Surprisingly, the major inhibitory effect of these two antagonists is similar, but additional more subtle differences are likely to distinguish the pharmacological profile of each. These findings provide new quantitative insight to the actions of two lineage-distinct SK inhibitors, and are likely to help guide future pharmacological targeting of SK channels in the heart, and perhaps other tissues.

Introduction

Calcium-activated potassium (K_{Ca}) channels are expressed across many tissues, and in all cases these channels link fluctuation of intracellular calcium to membrane potential dynamics and ionic homeostasis.[1,2] The K_{Ca} family consists of three independently cloned channels, encoded by separate genes and distinguished by characteristic divergence in sequence homology and unitary conductance: the large (BK; >200 pS, KCNMA1),[3] intermediate (IK; 50-100 pS, KCNN4)[4,5] and small conductance (SK; <20 pS, KCNN1/KCNN2/KCNN3)[1,6,7] channels. SK channels are the dominant K_{Ca} isoform expressed in the myocardium, and that expression is primarily atrial although some expression does occur in the ventricles and is thought to increase in certain disease conditions.[8–11] There are three SK subtypes (SK1/K_{Ca}2.1/KCNN1, SK2/K_{Ca}2.2/KCNN2 and SK3/K_{Ca}2.3/KCNN3), and SK2 and SK3 appear to be the dominant contributors to the human atrial SK population.[12]

The atria-specificity of SK channel expression provides a basis for chamber-selective pharmacological targeting, which is a major consideration for pharmacotherapy in atrial fibrillation (AF) - the most common cardiac arrhythmia.[13,14] Additionally, genome wide association studies and subsequent meta-analyses have suggested that variants in KCNN2 and KCNN3 (encoding SK2 and SK3) are involved in AF etiology.[15–17] Together, these characteristics have further pushed the SK family of channels to be among the front line molecular candidates for near-term AF pharmacotherapies. To that end, studies that have investigated the potential for SK channel targeting in AF have suggested that nonclinical inhibitors, such as NS8593 or ICAGEN, can exert an antiarrhythmic influence by prolonging the action potential (AP) in human atrial myocytes, without impacting the ventricular AP.[12] Clinical lineage compounds have now also shown promise, with some having reached human trials (e.g. AP30663: Acesion Pharma (Denmark).[18] These encouraging developments notwithstanding, relatively little is known about how the range of SK channel antagonists exert their effects on SK channel gating, and how these effects are likely to interact with the rapid calcium dynamics that regulate channel activity *in vivo*.

Activation of SK channels depends solely on intracellular calcium, and involves complex gating kinetics. The SK monomers have no intrinsic calcium-binding domain,[19] instead calcium interacts with the channel via calmodulin (CaM) constitutively bound to the intracellular C-terminal CaM Binding Domain (CaMBD). The activation sequence begins with calcium-CaM binding, followed by conformational changes within both CaM and its associated SK monomer, leading to a structural rearrangement of the pore-occluding domain to allow potassium ions to pass.[20–22] While relatively little single channel data is available to describe this activation sequence, it has generally been observed as a kinetic scheme involving three distinguishable closed durations, and two open durations.[23] Additionally, SK channel gating exhibits a clear modal property when data are averaged over longer periods (seconds), whereby channels shift between high and low open probability but retain the five distinct kinetic components.[23] Macroscopically, these effects cause channels, independent of SK isoform, to display a steep calcium

dependence with Hill coefficients ~3-5.[1,24] This differs from the Ca^{2+}-binding properties of free CaM, for which cooperativity is low, but is consistent with Ca^{2+}-CaM-mediated protein kinase and phosphatase activation, which involves two Ca^{2+} association events prior to CaM-binding.[25,26] This emphasizes a possible functional impact of the constitutive association between CaM and SK channels.[1,23]

Broadly speaking, SK channel inhibitors have been classified in terms of their impact on macroscopic properties of SK current. The early scorpion and bee venom peptide inhibitors (and their derivatives) bind such that the bulk of the molecule resides in the outer pore region of the SK channel. This was initially interpreted to indicate an inhibitory mechanism involving direct block of the potassium permeation path.[27] However, most currently known inhibitors have been classified (or reclassified) as negative modulators. This followed, in part, from observation that the bee-venom toxin, apamin (the prototypical SK selective inhibitor), acts via long range allosteric mechanisms rather than direct obstruction of the permeation path.[28–30] Subsequent studies, involving a range of peptide and small molecule inhibitors, suggested that allosteric effects on Ca^{2+}-CaM interaction or subsequent conformational changes in the activation sequence are the most common mechanisms of SK current inhibition.[21,28,31] A subclass of negative modulators, including AP14145, have shown antiarrhythmic properties in animal models and have also been shown to exert their modulatory effects by desensitizing SK channels to Ca^{2+}-activation in macropatch recordings.[32–38] While these studies have suggested a diversity and subtlety in the mechanisms of SK channel pharmacology, very few single channel data have been collected to directly characterize those mechanisms, either for apamin or indeed any negative modulator of SK channels. As such, our core objective was to quantitatively determine how apamin and AP14145 (a clinical lineage SK channel negative modulator developed by Acesion Pharma) impact single channel and macroscopic SK current.

We report that the major mechanism of inhibition by apamin and AP14145 results from infrequent but very long-lived channel closures. In the presence of AP14145, slower intra-burst gating kinetics and reduced amplitude was observed, while apamin induced shorter-lived intra-burst closures, most probably due in part to periods of flickery activity. Together, the long inter-burst channel closures and short intra-burst closures induced by apamin reduce SK current significantly by reducing overall open probability (P_o), while maintaining short periods of high intra-burst P_o. The multitude of effects induced by AP14145 reduced SK current even further by additionally reducing P_o within a burst, along with open channel amplitude. We conclude that apamin and AP14145 exhibit a similar dominant mechanism of inhibition, but more subtle differences in their impact on SK channel gating kinetics and unitary current amplitude emphasize the importance of small differences in their modulatory mechanisms.

Methods

Rat SK2 (rSK2) channel expression:

Recombinant rSK2 channels (GenBank accession number NM_019314) were transiently expressed in HEK293 cells. Cells were maintained in modified essential medium (DMEM, Invitrogen) supplemented with 10% fetal calf serum and 1% penicillin/streptomycin (Invitrogen) at 37°C. Cells were transfected using polyethylenimine (Alfa Aesar, Inc.) with rSK2 channels and enhanced green fluorescent protein (GFP, Invitrogen) using 1:10 plasmid ratio with maximal plasmid content of 1 µg. Only GFP-positive cells were used for single channel recordings, and these were made within 24 hours of transfection.

Solutions:

Patch clamp experiments were performed in symmetrical K^+ solutions, as for earlier characterizations of rSK2 single channel function.[1,23,39] The extracellular (pipette) solution contained (in mM) 97 K-aspartate, 30 KCl, 10 acid free HEPES, 10 EGTA, 1.44 $MgCl_2$ to a final Mg^{2+} concentration of 1 mM and 6.19 mM $CaCl_2$ to a final free Ca^{2+} concentration of 60 nM. Extracellular pH and osmolarity were adjusted with KOH to 7.4 and 280-300 mOsm, respectively. The intracellular solution differed from the extracellular solution in Mg^{2+} and Ca^{2+} concentrations (in mM): 1.04 $MgCl_2$ and 9.64 $CaCl_2$ were substituted to yield a free intracellular [Ca^{2+}] = 1 µM. This concentration is near-saturating in rSK2, but we chose it to approximate peak [Ca^{2+}] in the bulk cytosol of cardiac myocytes. We made this selection because SK2 is known to colocalize with L-type calcium channels (specifically Cav1.2 and Cav1.3) in heterologous systems (HEK), as well as both human and mouse native cardiac tissue.[40] Thus, suggesting that these channels experience elevated (Ca^{2+}) due to local microdomain effects, as has been observed in rabbit ventricular myocytes.[22] All reagents were obtained from Sigma-Aldrich. For pharmacological experiments, two different SK channel inhibitors were added to the extracellular (pipette) solution. Both were included at high concentration, as is common in the broader literature, and to provide the greatest chance of observing the active inhibitory mechanisms in these challenging recordings. In particular, apamin exhibits slow onset of inhibition (minutes timescale) near its IC_{50} of ~100 pM,[1,41] and thus was applied at 100 nM to overcome this limitation[42]. This apamin concentration also enables comparison with macroscopic SK recordings in clinically relevant populations, such as human atrial myocytes.[42]

AP14145 exhibits a macroscopic IC_{50} of ~1 µM in human SK2 with more rapid onset of inhibition, thus we applied it at 10 µM as in our prior macropatch assessments.[32] Apamin (Sigma Aldrich, UK) and AP14145 (Acesion Pharma, Denmark) solutions were prepared on the day of experiments from a frozen stock of 100 µM in water and 10 mM in dimethyl sulfoxide (DMSO), respectively. The final concentration of DMSO in the AP14145 containing solution was 0.1%. Calmodulin (CaM) is constitutively bound to the SK C-terminus and is responsible for conferring Ca^{2+}-dependence to SK channel gating.[19,43] We did not supplement the extracellular solution with exogenous CaM. This choice was made both to remain consistent with our prior SK single channel characterizations,[23,39] and because the degree to which SK monomers are saturated with endogenous CaM in atrial cardiomyocytes is not established.

Electrophysiology:
All recordings were performed on inside-out patches using thick-walled quartz electrodes pulled with a Sutter P-2000 pipette puller. In cell-attached configuration these pipettes resulted in seal resistances of 10-40 GΩ. Currents were recorded in voltage clamp mode with an Axopatch 200A (MDS Analytical Technologies), coupled to a CV201A head stage. All recordings were made at a constant holding potential of -50 mV (expressed conventionally as intracellular minus extracellular). We chose this potential as it is in the linear range of the mildly inwardly rectified SK current. It thus facilitates interpretation of changes in unitary amplitude at a single potential, while also offering a reasonable compromise between signal-to-noise (for these small conductance channels) and seal stability. In addition, our previous study showed no difference in kinetics components at -50, -60 or -100 mV.[23] Data were filtered at 1 kHz (eight-pole Bessel; Frequency Devices, Inc.), acquired at a sample interval of 100 µs using Pulse software (HEKA Elektronik), and stored. Experiments were performed under steady-state conditions with solutions and pharmacological compounds continuously present during the recording and at least 1 minute before data acquisition. All experiments were performed at room temperature (20-25°C).

Single channel analyses:
Single channel transitions were analyzed via TAC software (X4.3.3, Bruxton), based on the 50% threshold technique and visual inspection, as previously reported.[23,39] Data were analyzed by one of two trained analysts and, importantly, the same fraction of recordings was analyzed by each for all experimental groups. Single channel amplitudes were fit only to events > 1 ms to eliminate artifacts resulting for the rise time of the Bessel filter. Durations were visualized as logarithmically binned histograms (18 bins per order of magnitude in time), whereas amplitude histograms were linearly binned (10 bins per 0.1 pA) using TACFit. The histograms were fitted with separate probability density functions (pdfs) for amplitude (Gaussian), open duration and closed duration (exponential), using the maximum likelihood method. The duration pdf for a distribution consisting of N exponentials is:

$$f(t) = \sum_{i=1}^{N} \frac{a_i}{\tau_i} e^{-t/\tau_i}$$

where τ_i is the duration and a_i is the weight of the *i*-th term.

After log transformation:

$$g(x) = \sum_{i=1}^{N} a_i g_0(x - ln\tau_i)$$

where $x = \ln(t)$, $g_0(x) = exp[x - \exp(x)]$ and a_i is the weight of a given term. Parameters a_i and τ_i were varied by Powell's method in the maximum likelihood fitting for a variable number of components (*i* = 1,2… *n*).

For amplitude pdfs, the distribution consisting of a sum of *n* Gaussians is:

$$f(x) = \sum_{i=1}^{n} \frac{a_i}{\sigma_i\sqrt{2\pi}} exp\left[-\frac{(x - A_i)^2}{2\sigma_i^2}\right]$$

where f(x) is the total probability density of amplitude x, which can be described by fitted components (i = 1,2… n). A_i is the i-th amplitude, σ_i is the standard deviation of the i-th amplitude, and a_i is the fraction of events exhibiting the i-th amplitude. The parameters a_i, A_i and σ_i were again varied by Powell's method in the maximum likelihood fitting.

Gaussian distributions were required to exhibit equal variances, and a minimum 3-fold separation of the exponential components was applied as an *a priori* constraint.[44] All components were assigned to a respective amplitude or duration class (A_i , τ_i). For patches in which the number of fitted components (n) in an amplitude or duration histogram was less than the maximum n, the components of that histogram were assigned to the component class (e.g. low or high amplitude) with the closest mean value from the patches that included all components. For amplitude and open duration, these procedures resulted in the probability density functions (pdfs) used for all further analyses. Closed duration histogram analyses consisted of an additional step.

It is common for patches containing multiple channels to be excluded from closed-duration analyses because it is not possible to identify which of the identical channels is active. However, individual channel openings separated by short closures most likely result from bursting behavior of a single channel.[45,46] Thus, we assumed that intra-burst kinetics represent the behavior of only one channel even in patches containing multiple channels.[47,48] Bursts with simultaneous multi-channel openings were not analyzed. Through this approach we were able to analyze the gating kinetics within (from both single- and multi-channel patches) and between bursts (single-channel patches only). Hirschberg et al [23] observed 3 closed durations, with events in the longest closed duration class separating bursts of activity. Thus, for this burst analysis we assumed that the two shortest (later called short and intermediate) closed durations occur within a burst, while longer duration components separated bursts. Through decomposing the dataset in this way it was possible to observe unique characteristics of the inter-burst closed duration distributions. In the cases of apamin and AP14145, these inter-burst periods exhibited a number of very long channel closures (often > 10 s). For this reason, single channel experiments shorter than 10 s were excluded from inter-burst analyses for all groups i.e. because the longest closed duration (> 10 s for apamin and AP14145) would not be observable during the experiment.

To formally assign each closed event to an intra- or inter-burst period, a burst delimiter (t_d) was calculated for each experimental group (control, apamin and AP14145). Defining burst delimiters in this group-specific manner was deemed necessary due to unknown kinetic effects of the inhibitors. To calculate these three burst delimiters, all closed events from single channel experiments lasting longer than 10 s were combined for each experimental group. The resulting three histograms were fitted with the number of

components determined by maximum likelihood, which yielded three closed durations for control and four closed durations for both the apamin and AP14145. From these group-level fits, the t_d value for each group was then calculated from the 2nd and 3rd closed duration components (the intermediate, $\tau_{c,i}$, and long, $\tau_{c,l}$, closed durations, respectively) via:

$$1 - e^{-\frac{t_d}{\tau_{c,l}}} = e^{-\frac{t_d}{\tau_{c,i}}}$$

This expression equalizes the proportion of intervals classified incorrectly as either intra- or inter-burst, and is easily solved for t_d.[47] Once t_d was calculated for each experimental group, the intra-burst and inter-burst data for each patch were separately subjected to maximum likelihood fitting. The intra-burst closed events were fitted for two components - the short closed duration, $\tau_{c,s}$, and $\tau_{c,i}$, respectively. The inter-burst data were fitted for either one ($\tau_{c,l}$) or two ($\tau_{c,l}$ and $\tau_{c,vl}$, the very long closed duration) components depending on whether or not drug was present.

Table 1 provides a comprehensive overview of the number of recordings contributing to each of these analyses, and the resulting characteristics for each of the three experimental groups. All data and analysis code for reproducing each figure will be publicly accessible here.

Data Reduction and Statistical inference:

To better visualize the influence of rare gating events with very long closed times, diary plots were constructed from the tables of tracked events and show the channel behavior over the full length of the recording. Bin-width for these analyses was chosen to be 0.1 s, which is between the observed $\tau_{c,i}$ and $\tau_{c,l}$ for all groups. We also use the "occurrence" of each amplitude or duration component in each experimental group to describe how commonly each of those components was observed in the three experimental groups. This was calculated as the proportion of patches exhibiting that component divided by the total number of patches in the corresponding group.

Summary results are presented as means ± SEM. Data for each amplitude level, and each open and closed duration were subjected to separate 1-factor ANOVAs. The Bonferroni correction was applied for conservative type 1 error protection of all parametric *post hoc* comparisons. In all cases the correction was applied family-wise (n = 3 multiple comparisons) to cover all possible pairwise comparisons. Proportion values in diary plots, and occurrence values for the two amplitude levels and each kinetic component, were separately examined by the Chi-square test. In all cases, the threshold for type 1 error was set at $\alpha = 0.05$.

Results

Single SK2 channel gating kinetics and unitary current amplitudes

At a constant voltage (as applied here) the amplitude of single SK2 channel openings is indicative of single channel conductance. Our recordings of single rSK2 channels indicate two distinct amplitude components in 75% of control patches (Figure 1A-B), which has not been reported in previous studies of these channels. Direct transitions between amplitude classes were observed in both directions (up- and downward arrows in Figure 1B) without requiring

channel closure, which strongly suggests that these events represent transition between conductance states of a single channel. Figure 1C depicts exemplary amplitude (left), and open duration (right) distributions for all events from a single control patch. At -50 mV, 12 of 16 control patches exhibited both high (A_{high}) and low (A_{low}) amplitude components (Figure 1D). For the remaining 4 patches the single amplitude values were closest to the mean A_{high}, and thus were also designated as A_{high} (see Methods). On average, A_{low} was 71% of A_{high}, and as is expected from the maximum likelihood criteria, this difference easily reached significance (-0.538 ± 0.033 pA vs. -0.758 ± 0.033 pA, $p < 0.001$). Importantly, we found no differences in the open duration distributions upon separating the two amplitude classes (Figure 1E-G). Figure 1E shows the open duration distributions (right) for subsets (classes) of the opening events (left), with either high amplitude (top) or low amplitude (bottom). Both high and low amplitude events could be fit with two mean open durations, and those durations were not different for the two amplitude classes (Figure 1F), Because many events had to be excluded when separating the overall distribution into only high or low amplitude events, we also asked whether there was any correlation between open duration and amplitude across all events. We found none, as depicted for one exemplary recording in Figure 1G, again suggesting that channel open duration is independent of amplitude in rSK2 channels. For this reason, we grouped both amplitude classes together for further analysis of open duration kinetics.

The broader kinetic profile for our control recordings (Figure 2) is very similar to previous reports of rSK2 channel gating.[23] As mentioned above, control open duration histograms were best-fitted with a two-component probability density function (Figure 2A). The mean short ($\tau_{o,s}$) and long ($\tau_{o,l}$) open durations were 4.0 ± 0.1 ms (n=16 patches) and 34.8 ± 9.3 ms (n=14 patches), respectively. The shorter open duration also comprised a larger fraction of total events in control patches (62 ± 6 % in $\tau_{o,s}$, vs. 38 ± 6 % in $\tau_{o,l}$). It is noteworthy that both open durations presented here are ~3-4 fold longer than the durations at $[Ca^{2+}]$ = 1 μM presented by Hirschberg et al.[23] This is likely due to differences in identification of short open events assessed by the two different analysts, as all other procedures remained identical including hardware and filtering. Our prior studies suggest that rSK2 channels gate with 3 distinguishable closed durations,[23] and here we have again observed 3 closed durations in the majority of control patches (Figure 2D-E). The mean short ($\tau_{c,s}$) and intermediate ($\tau_{c,i}$) closed durations were 1.59 ± 0.19 ms (n=16 patches) and 13.5 ± 1.2 ms (n=16 patches), respectively. As described above, we applied burst analysis to decompose bursts of single channel activity in multi-channel patches. The burst delimiter value for control patches, which defines the maximum time a channel can remain closed within a bursting period,[46] was 31.8 ms. As expected, most events occurred during burst periods, whereas the inter-burst periods yielded a much smaller number of longer duration closures. In control recordings only one component could be fitted to the inter-burst closed duration distributions. This long closed duration ($\tau_{c,l}$) averaged 132.4 ± 18.8 ms (Figure 2F). Because this approach necessitated rigorous constraint on the inter-burst data (single-channel patches each of at least 10 s duration), only 4 of the 16 control patches were analyzed for inter-burst kinetics.

Apamin does not alter open channel behavior, whereas AP14145 reduces rSK2 channel unitary current amplitude but promotes longer duration openings

While apamin did not alter either amplitude or open duration, AP14145 both reduced unitary current amplitude and slightly shifted the open duration distribution towards long opening events. Figure 3A shows a typically narrow and left-shifted representative amplitude distribution for AP14145 relative to apamin (and control, comparison shown in Figures 3A and 3B). Figure 3B depicts the more similar (to each other) open duration distributions for the two negative modulators. At the summary level, the fraction of patches exhibiting each amplitude was unchanged by apamin, whereas only 4 of 9 AP14145 patches could be fit with a high amplitude component (Figure 3C, $p < 0.001$). The means of both amplitude components for apamin were not different from control (A_{low} = 0.54 ± 0.04 pA and A_{high} = 0.74 ± 0.04 pA; both $p > 0.05$ vs. control, Figure 3D), although apamin did occasionally induce long, low amplitude openings (Figure 4A). While these events were visually striking, they proved very rare in the complete dataset, and thus were not sufficient to alter the summary results. In contrast, AP14145 did reduce the mean low amplitude (0.38 ± 0.03 pA; $p < 0.05$ vs. control, Figure 3D), but interestingly left the higher amplitude class unaffected (0.58 ± 0.06 pA, $p > 0.05$ vs. control, Figure 3D). Similar to the amplitude results, apamin did not alter either the occurrence (Figure 3D) or mean open times ($\tau_{o,s}$ = 3.6 ± 1.0 ms, and $\tau_{o,l}$ = 20.9 ± 3.6 ms; both $p > 0.05$ vs. control, Figure 3F). AP14145 subtly shifted the occurrence of the open time distribution to favor longer open times. That is, the number of patches exhibiting short duration openings was reduced in the presence of AP14145 (6/9 patches) vs. control, (16/16 patches), $p < 0.05$ (Figure 3E). Neither the mean open times ($\tau_{o,s}$ = 4.6 ± 0.8 ms, and $\tau_{o,l}$ = 36.6 ± 11.5 ms, both $p > 0.05$ vs. control, Figure 3F), nor the relative weighting of each component ($\tau_{o,s}$ = 42 ± 14 %, $p > 0.05$ vs. control, Table 1), were altered by AP14145. A complete overview of these amplitude characteristics and both the open- and closed-state durations is presented in Table 1. Together these data suggest that AP14145 acts to reduce whole-cell SK current at least in part by reducing the amplitude of single channel openings, and preventing the larger amplitude openings observed in untreated channels. Both effects will, however, be at least partially counteracted *in vivo* by longer duration openings in the presence of AP14145. In contrast, it does not appear that apamin consistently alters the function of open rSK2 channels. However, it is worth noting that we did occasionally observe openings in the presence of apamin that were striking in that they were both prolonged and of low amplitude (Figure 4A).

Apamin and AP14145 exert opposite effects on intra-burst closed channel kinetics

In contrast to the open channel dynamics (gating kinetics and unitary current amplitudes), both apamin and AP14145 induced pronounced changes to the rSK2 channel closed duration distributions. As mentioned in the methods, by applying burst analysis we are able to discriminate the rapid closed duration components (intra-burst kinetics) of single channels within multi-channel patches. The major effects of apamin and AP14145 on the intra-burst closed

channel kinetics are depicted in representative single channel recordings (Figure 4A) and representative closed dwell-time distributions (Figure 4B). Both apamin and AP14145 shifted the mean values of both the short ($\tau_{c,s}$) and intermediate ($\tau_{c,i}$) closed durations. This can be seen both in the representative distributions (Figure 4B) and the summary data (Figure 4D). Figure 4B shows that both components of the intra-burst durations (bold line) are left-shifted for apamin and right-shifted for AP14145, as are the corresponding burst delimiters. These effects were consistent and pronounced (Figure 4D). Apamin reduced both $\tau_{c,s}$ (0.75 ± 0.10 ms; $p < 0.01$ vs. control) and $\tau_{c,i}$ (5.08 ± 0.49 ms; $p < 0.01$ vs. control) to less than half the corresponding control durations ($\tau_{c,s}$ = 1.59 ± 0.19 ms and $\tau_{c,l}$ = 13.5 ± 1.2 ms). Conversely, AP14145 approximately doubled both durations ($\tau_{c,s}$ = 3.50 ± 0.81 ms; $p < 0.05$ vs. control, $p < 0.001$ vs. apamin; $\tau_{c,i}$ = 32.0 ± 6.76 ms; $p < 0.01$ vs. control, $p < 0.001$ vs. apamin). Neither apamin nor AP14145 altered the ability to fit two closed dwell times to the intra-burst distributions (Figure 4C) – intra-burst periods for all but one AP14145 recording (of 9) were best fit with two closed dwell times. Interestingly, the effect of apamin may have been partially due to induction of periods in which channels appeared to exhibit rapid sustained transitioning between conducting and non-conducting states (depicted as flickery activity in Figure 4A). While these episodes were not common enough to introduce additional distinguishable kinetic components in either the closed or open duration distributions, they may represent a distinct form of apamin-mediated modulation. To formally investigate the prevalence of the periods of flickery activity, we assessed the fraction of time that was spent in contiguous sequences of events for which each closed event was less than 5 or 10 ms duration, and each open event less than 1 ms. We performed this analysis for sequences including at least 10 events, 20 events, or 40 events, and present these results in Table 2. We observed that apamin uniquely increased the fraction of time spent in thus-defined flickery activity using all versions of the defining criterion. This flickery mode accounted for between 3% (for 20 sequential events, closed times < 5 ms) and 14% (10 sequential events, closed times < 5 ms) of the total recording time that remained after subtracting the large portion of time spent in the very-long channel closures. This suggests that this type of activity may be a unique modulatory action of apamin.

Both apamin and AP14145 induce very long channel closures

In the absence of inhibitor, single rSK2 channels exhibit modal gating (distinct from the apamin-induced flickery activity described above), where channels transition between relatively long-lived periods of high and low P_o.[23] Each mode is characterized by distinct single channel kinetics, for which low P_o periods exhibit a long closed duration approximately an order of magnitude longer than high P_o periods. Both modes still exhibit the same number of open and closed duration components. The fraction of time spent gating in high P_o-mode is steeply dependent on cytosolic [Ca^{2+}] in the physiologic range (EC_{50} = 0.52, Hill coefficient = 4.1).[23] At the 1 μM [Ca^{2+}] used herein, this modal property is nearly saturated such that approximately 90% of all gating is in high P_o-mode.[23] Our prior work suggests that the long closed duration ($\tau_{c,l}$) ranges between approximately 25 and 60 ms in this mode, as compared with 250-2000 ms in low P_o-mode.[23] As shown in Figure 2F, our control recordings

at 1 μM [Ca^{2+}] exhibit a mean long closed duration of 132 ± 19 ms, which likely indicates some mixing of low P_o-mode behavior. To discriminate closures longer than approximately 500 ms requires long recording periods, and because they are relatively infrequent events (but functionally important), such long closures are not easily visualized in the closed duration distributions with more frequent and short-lived intra-burst closed events. Instead, closures on the time-scale of seconds can be observed as non-uniformities in diary plots of time-varying P_o. We present these trajectories as P_o frequency histograms (0.5 s binning duration) in Figure 5A. Here we observe some non-uniformity in the control recordings, however, the outstanding result is that both apamin and AP14145 induce pronounced periods of very low (or zero) P_o on the seconds-to-minute timescale, which alternate with brief periods of high activity (Figure 5A, middle and bottom panels). These observations strongly suggest that both inhibitors induce very long channel closures, or prolonged periods of very low channel activity.

To assess this possibility in more detail, we analyzed the inter-burst closed durations in recordings with only one channel, and of at least 10-s total recording time (to allow discrimination of such long events). These analyses are shown in Figure 5B-D, and suggest that the drug-induced shifts observed in the diary plots most likely result from a class of very long closed events not present in control recordings. All patches treated with apamin and AP14145, required a second inter-burst closed duration component, which we termed the very long closed duration ($\tau_{c,vl}$), to fit this class of very long-lived closed events (Figure 5C). Because only long recordings of single-channel patches could be used for inter-burst analyses, and the number of such patches was quite small (n=4 for control and apamin, and n=3 for AP14145), our power for conducting formal statistical inference is relatively modest. Still, applying Chi-square tests suggests that both apamin and AP14145 induced a separate class of closed events (3/3 channels, both $p = 0.014$ vs. control 0/3 channels, Figure 5C). This very long kinetic component reflected mean closed times of 11.8 ± 7.1 s (apamin) and 10.3 ± 7.2 s (AP14145). The other inter-burst closed duration, $\tau_{c,l}$, was present in both apamin and AP14145 recordings, but was not different to control (both $p > 0.05$). As described further in the discussion, we have not conducted a formal concentration-response to characterize the concentration dependence of this very-long closed duration. However, we can approximate on-rates for each drug by assuming that the K_d for this class of events is similar to the macroscopic K_d's. For apamin we use 5 pM.[28] For AP14145, we use as proxy the K_i (550 nM) calculated from the Cheng-Prusoff equation (applying the AP14145 IC_{50} measured at 400 nM Ca^{2+}).[32] Applying this approach and the corresponding $k_{off} = 1/\tau_{c,vl}$ for apamin we calculate an apparent k_{on} at 100 nM of 1.7 x 10^7 s^{-1} and intrinsic k_{on} of 1.7 x 10^{11} $mM^{-1}.s^{-1}$. Proceeding similarly for AP14145, the apparent and intrinsic on-rates are 177 s^{-1} (at 10 μM) and 1.77 x 10^4 $mM^{-1}.s^{-1}$, respectively.

Table 1 includes an explicit accounting of the importance of these very long (VL) closed events to overall inhibition by both drugs. There we applied two thresholds for counting a closure as a VL event (events longer than either 1s or 2.9s). The 1-second threshold is approximately 10-fold longer than the mean long closed duration for control patches, and 2.9-seconds was the

duration of the longest single closed event in a control patch. In either case we observed much greater prevalence of the VL events in both AP14145 and apamin. Further, the average fraction of recording time spent in closures > 2.9s was 66% for apamin and 49% for AP14145 (control = 0%). If we pooled all events together (rather than averaged per patch), the effect was even more pronounced at 86% of total recording time for apamin and 62% for AP14145. Applying the 1s threshold, these values were 93% for apamin, 75% for AP14145, and 34% for control. Many tens of these VL events contributed to these effects for both apamin and AP14145, and they occurred at significantly higher frequency (Table 1). Together, these observations make a compelling argument that these long events are the major mechanism of inhibition for both AP14145 and apamin.

To assess the possibility that there is some mode-specificity for induction of these very long closures by either apamin or AP14145 we analyzed segments of 500 ms before and after VL closures longer than 1 s and 2.9 s. Periods before and after closures showed no bias towards low or high P_o behavior for either drug, nor were there any differences between drugs for the P_o directly preceding or after VL closures (all $p > 0.05$, Table 1). This suggests that induction of the very long closed events is not more easily entered from a conformation promoting either P_o-mode behavior.

Together, these analyses strongly suggest that the major mechanism by which both apamin and AP14145 inhibit rSK2 channels is through induction of very long non-conducting events.

Discussion

We have examined the impact of two SK channel inhibitors (apamin and AP14145) on the dynamic properties of rSK2 channel gating in single channels. Both compounds are well known to selectively and potently inhibit SK-mediated currents, and both are thought to exert their inhibition as modulators of channel gating rather than by directly blocking the ion permeation path.[28,29,32,33] However, the molecular bases for these effects are very likely to be distinct. Apamin is the prototypical peptide inhibitor of SK2 current first isolated from western honey bee venom,[49] whereas AP14145 is a clinical lineage small molecule developed by Acesion Pharma in pursuit of new and selective treatments for atrial fibrillation.[32,33] Available structural data suggest that their inhibitory actions occur via distinct allosteric mechanisms.[28,29,32,33] For these reasons we sought to determine if such differences manifest at the level of single SK2 channel dynamics, and may therefore provide a basis for predicting *in vivo* cardiac pharmacodynamic responses.

The major mechanism of apamin and AP14145 inhibition is induction of very long-lived channel closures

At the single channel level, both inhibitors exert their major influence on SK channel function by introducing a new very long closed duration, which was never observed under control conditions. This very long closed duration separates periods of channel activity with prolonged periods of apparent quiescence that last from several seconds to several tens of seconds. The

resulting reduction in overall channel activity would be expected to reduce the macroscopic SK current by up to 98% under conditions approaching saturating Ca^{2+} activation. It should be noted that this major finding is somewhat complicated by the modal behavior intrinsic to normal SK channel gating (in the absence of inhibitor), where shifts from high to low activity are accompanied by a change in the long closed duration of approximately an order of magnitude (30 to 300 ms, at 1 μM Ca^{2+}).[23] However, we contend, for two reasons, that the very long closures observed in the presence of either apamin or AP14145 are unambiguously different from this mode-shifting, and do not simply reflect an effect of the drugs to promote the low activity regime. First, the very long closed durations range from one to three orders of magnitude longer than the longest closed duration observed under control conditions herein, and in low P_o-mode previously.[23] Second, diary plots (Figure 5A) suggest that, while our relatively high (1 μM) Ca^{2+} conditions do shift gating kinetics towards the high-activity regime, both P_o-modes are likely still present. Therefore, this mechanism of inhibition is likely to be independent of modal gating shifts, and both P_o-modes occur in presence of the inhibitors. We also observed that both apamin and AP14145 can induce long channel closures during both low and high activity periods. AP14145 showed multiple effects on channel activity not included in this analysis of P_o-mode specificity (e.g. changes to unitary amplitude and intra-burst kinetics). A second important note is that these effects were observed at relatively high concentrations of both drugs. AP14145 was applied at concentration that elicits between 50% and maximal inhibition (depending on $[Ca^{2+}]$),[32] and apamin was applied at supra-maximal (>IC_{99}) inhibitory concentration. It would be desirable to understand the effect of differing drug concentrations on the length (or prevalence) of these very long closures, however the patch-to-patch variability of $\tau_{c,vl}$ causes that assessment to constitute a tremendous experimental undertaking. Rudimentary power calculations suggest that approximately 50 recordings meeting all criteria would be required to discern even a relatively large (~50%) concentration-dependent change in $\tau_{c,vl}$. Given that few (~30%) of all recordings met the criteria for $\tau_{c,vl}$, the total number of recordings would be well in excess of 100 patches. The similarity between apamin and AP14145 in this major mechanism of inhibition is surprising. However, we have no evidence that the molecular mechanisms are common for the two drugs, and caution against such a conclusion. Indeed, given prior reports that the primary association domains are distant and on opposite sides of the membrane, considerable further investigation would be required to establish a common downstream mechanism.[28–32,41] Apamin, in part due to the fact that it inhibits the channel from the extracellular side,[29] was initially assumed to be a pore-blocker. However, site-directed mutagenesis, homology modeling, and poly-pharmacology studies have indicated that it has two binding sites, in the outer pore[28–30] and the S3-S4 extracellular loop of a neighboring subunit within the channel tetramer.[29] Given apamin's small size (18 amino-acids), and the observation that the binding site closest to the channel pore exists in the S5-PHelix loop (outer pore region) of the SK monomer,[28] it is geometrically incapable of directly obstructing the permeation path. In contrast, the structural basis for AP14145 inhibition appears far removed from apamin. Displacement experiments have shown that NS8593 (a structural analog of AP14145) does not share an interaction site with

apamin, but rather binds in the inner pore vestibule of the SK channel.[34,38] Furthermore, both AP14145[32] and its structurally similar precursor (NS8593)[35,38] reduce SK channel calcium sensitivity and inhibit the channel via an allosteric mechanism. This effect represents negative modulation, and is liable to being reversed through competition from the positive modulator (calcium sensitizer) NS309.[32] These functional data suggest that AP14145 exerts a dominant mechanism of inhibition via altering calcium-dependent activation, but that multiple mechanisms may be important.

To our knowledge, external Ba^{2+} is the only other inhibitor known to induce such long K^+ channel closures. Ba^{2+} block is ubiquitous across many K^+ channel families, and thought to reflect direct block of permeation through sites in the pore and particularly the selectivity filter.[50] The time course of Ba^{2+} block often exhibits multiple components.[51] The ability for Ba^{2+} to elicit very long closures has been reported for BK channels, where mean closed durations are in the range of several seconds (~1-4), depending on internal and external K^+ concentration and membrane potential.[52–55] Even longer Ba^{2+} blocking events occur Shaker K^+ channels, where 2 mM external Ba^{2+} induces closures that can last several tens of seconds.[56] It is possible that Ba^{2+}-induced events of this duration occur in other classes of K^+ channel, but have not been reported due to the requirement for long recording durations, which are challenging in many single channel preparations.

In summary, our observation that AP14145 and apamin elicit a similarly long-lived non-conducting state of the SK2 channel suggests an unexpected commonality in the major outcome of inhibition for these two compounds. All available data indicate that the structural bases for these two effects are distinct, which in turn suggests that some common downstream allosteric outcome may be responsible for the inhibition resulting from these two very different classes of SK channel antagonist. Whatever the molecular events are that underlie those outcomes, it appears that they are the only significant mechanism for inhibition by apamin (although other modulatory effects are apparent), whereas both this and prior studies suggest that AP14145 may exhibit multiple mechanisms of inhibition. Certainly, the very long closures induced by AP14145 were the most powerful form of inhibition we observed for AP14145 inhibition, but this was not the only important mechanism in the complex changes to SK channel gating we have observed for AP14145.

AP14145 slows whereas apamin accelerates intra-burst gating kinetics

In addition to inducing very long duration closed events separating bursts, both apamin and AP14145 impacted gating kinetics within bursts. The duration of channel openings were not affected by AP14145, but the occurrence of the short opening events was significantly reduced, thus shifting the balance toward longer open durations. This subtle effect would be expected to result in a modest increase in SK channel activity *in vivo*, but is greatly overshadowed by the cumulative effect of AP14145's other actions, all of which reduce macroscopic SK current. The closed durations within a burst (short and intermediate time constants) were prolonged by AP14145 but markedly abbreviated by apamin, which also appeared to induce occasional episodes of flickery activity, and similarly rare but prolonged low amplitude

openings. We have no direct evidence that either of these behaviors were due to a direct blocking mechanism, and may reflect forms of modulatory mode-shifting. Together, the longer intra-burst closed durations and the greater prevalence of long open durations, result in slower overall intra-burst gating in the presence of AP14145. Because apamin did not alter the mean open dwell times, it is likely that its abbreviation of intra-burst channel closures (in part due to flickery activity) counteracts its major inhibitory effect of inducing very long inter-burst closed events.

Only AP14145 impacts unitary current amplitude

We have observed that single SK channels can open in two different amplitudes classes, and in this dataset each class occurred with approximately equal prevalence. While we have not conducted formal current-voltage relationships to assess the slope conductance of each class, those calculated from the average amplitudes were 10.8 pS and 15.2 pS. Due to the small conductance of the SK channel and the small difference between the low and high conductances, it is not surprising that the difference in amplitudes has not been reported yet. The SK channel is commonly functionally identified by a unitary conductance < 20 pS, with most observations in the range 4-14 pS in symmetrical potassium. Both amplitude classes displayed identical open duration kinetics, and event amplitude was not correlated with kinetic behavior of the SK channel. Due to the similarity in open state kinetics and direct transitions between amplitude classes, it is most likely that the low amplitude openings represent a sub-conductance state of the open rSK2 channel.

Apamin had no effect on SK channel amplitude at -50 mV and $[Ca^{2+}]$ = 1 μM, either in terms of their absolute values or relative prevalence. In contrast, AP14145 decreased the occurrence of the high amplitude and the absolute value of the low amplitude events. This adds another mechanism of inhibition attributable to AP14145. Viewing this mechanism from a structural perspective, two residues (S508 and A533 for rSK3; S507 and A532 for hSK3) in the inner pore of SK3 channels confer sensitivity to NS8593 as well as AP14145.[32,34] Mutating corresponding residues in the NS8593-insensitive IK channel pore (to match the NS8593-sensitive SK3 channel) transfers both the interaction site and potent inhibition observed for SK3 channels, but confers a form of inhibition that is much less calcium- and NS309-sensitive.[34] This suggests that these residues permit a form of inhibition that resembles pore-block, rather than negative modulation.[34] This partial pore-block mechanism is also supported by the mechanism of IK block via TRAM-34. The sensitivity of IK channels to TRAM-34 is mediated by the same sites in the pore region of the SK channel for NS8593 and AP14145 binding.[21,34,57,58] However, while molecular modeling of TRAM-34 suggests that it coordinates among all four subunits to fill the site that would ordinarily be occupied by K^+ in the IK permeation pathway, NS8593 only coordinates with two adjacent subunits in a binding pose that is not expected to completely block permeation.[21,34,58] Together, the similarity in binding site and mechanism of TRAM-34 makes it reasonable to expect that NS8593 (and perhaps AP14145) partially obstruct the SK channel pore, although this clearly requires further interrogation. With respect to AP14145, we have at least observed a reduced

frequency of high amplitude SK channel openings as well as reduced amplitude in the low amplitude class. This would be expected to contribute a component of inhibition that is calcium independent, and additional to the modulatory effects observed as changes to gating kinetics that are known to be calcium dependent.

Conclusions and Limitations

We have applied single channel patch clamp to elucidate the pharmacological effects of two developmentally distinct negative modulators on the complex gating kinetics of the SK channel. First, in the absence of inhibitors, we have extended our prior rSK2 channel characterizations[23] by observing that open channels exhibit two amplitudes with identical open-state kinetics. Most importantly, and unexpectedly, we have demonstrated that (at the level of channel gating kinetics and unitary current) the major inhibitory outcome is similar for apamin and AP14145. Both compounds inhibit SK current by inducing long channel closures (> 10 s), the like of which are never observed in control recordings. This induction of long periods of inactivity was the only observed inhibitory effect of apamin on SK channel gating, although it also introduced counteractive shortening of closures during bursts of channel activity. In contrast, AP14145 elicited multiple inhibitory effects. Similar to apamin, very long closures constituted the primary mechanism of AP14145 inhibition, but this combined with prolonged intra-burst closed durations and reduced unitary current. All of these three effects would result in a reduced SK current, but the combination illuminates the complexity and potency of AP14145's inhibitory actions. These data clearly demonstrate unique dynamic modulation of these channels by both drugs, with implications for their effects *in vivo*. Integrating these observations through quantitative computational models of SK kinetics will permit a comprehensive mechanistic interrogation of both compounds in excitable cells and will be a high priority for future studies.

Author Contributions

IvH collected and analysed data, and wrote the manuscript. VS collected data, performed analyses, and critically reviewed the manuscript. BB contributed to design of the study, and critically reviewed the manuscript. NM contributed to design of the study, collected and analysed data, and critically reviewed the manuscript. AE contributed to design of the study, analysed data, and wrote the manuscript.

Declaration of Interest

BB is an employee of, and has financial interest in, Acesion Pharma ApS, a developer of SK targeting compounds including AP14145. Other authors declare no competing interests.

Acknowledgements and Funding

IvH and BHB received funding from the European Union's Horizon 2020 research and innovation programme under the Marie Sklodowska-Curie grant agreement number 675351. VS was supported by grant 9.4560.03 from the FNRS (Belgium). NVM has received funding from the British Heart Foundation

under agreement number PG/16/37/31974. AGE was supported by the Norwegian Ministry of Research and Education through the SUURPh international doctoral program.

References

1. Köhler, M. *et al.* Small-Conductance, Calcium-Activated Potassium Channels from Mammalian Brain. *Science* 273, 1709–1714 (1996).

2. Stocker, M. Ca2+-activated K+ channels: molecular determinants and function of the SK family. *Nat Rev Neurosci* 5, 758–770 (2004).

3. Pallanck, L. & Ganetzky, B. Cloning and characterization of human and mouse homologs of the Drosophila calcium-activated potassium channel gene, slowpoke. *Hum Mol Genet* 3, 1239–1243 (1994).

4. Ishii, T. M. *et al.* A human intermediate conductance calcium-activated potassium channel. *Proc National Acad Sci* 94, 11651–11656 (1997).

5. Joiner, W. J., Wang, L.-Y., Tang, M. D. & Kaczmarek, L. K. hSK4, a member of a novel subfamily of calcium-activated potassium channels. *Proc National Acad Sci* 94, 11013–11018 (1997).

6. Chandy, K. G. *et al.* Isolation of a novel potassium channel gene hSKCa3 containing a polymorphic CAG repeat: a candidate for schizophrenia and bipolar disorder? *Mol Psychiatr* 3, 32–37 (1998).

7. Blatz, A. L. & Magleby, K. L. Single apamin-blocked Ca-activated K+ channels of small conductance in cultured rat skeletal muscle. *Nature* 323, 718–720 (1986).

8. Xu, Y. *et al.* Molecular Identification and Functional Roles of a Ca2+-activated K+ Channel in Human and Mouse Hearts*. *J Biol Chem* 278, 49085–49094 (2003).

9. Tuteja, D. *et al.* Differential expression of small-conductance Ca2+-activated K+ channels SK1, SK2, and SK3 in mouse atrial and ventricular myocytes. *Am J Physiol-heart C* 289, H2714–H2723 (2005).

10. Li, N. *et al.* Ablation of a Ca2+-activated K+ channel (SK2 channel) results in action potential prolongation in atrial myocytes and atrial fibrillation. *J Physiology* 587, 1087–1100 (2009).

11. Zhang, X.-D. *et al.* Critical roles of a small conductance Ca2+-activated K+ channel (SK3) in the repolarization process of atrial myocytes. *Cardiovasc Res* 101, 317–325 (2014).

12. Skibsbye, L. *et al.* Small-conductance calcium-activated potassium (SK) channels contribute to action potential repolarization in human atria. *Cardiovasc Res* 103, 156–167 (2014).

13. Nattel, S. & Dobrev, D. Controversies About Atrial Fibrillation Mechanisms. *Circ Res* 120, 1396–1398 (2017).

14. Martignani, C., Massaro, G., Biffi, M., Ziacchi, M. & Diemberger, I. Atrial fibrillation: an arrhythmia that makes healthcare systems tremble. ***J Med Econ*** **23, 1–3 (2020).**

15. Ellinor, P. T. ***et al.*** **Common variants in KCNN3 are associated with lone atrial fibrillation.** ***Nat Genet*** **42, 240–244 (2010).**

16. MOHANTY, S. ***et al.*** **Variant rs2200733 on Chromosome 4q25 Confers Increased Risk of Atrial Fibrillation: Evidence From a Meta-Analysis.** ***J Cardiovasc Electr*** **24, 155–161 (2013).**

17. Christophersen, I. E. ***et al.*** **Large-scale analyses of common and rare variants identify 12 new loci associated with atrial fibrillation.** ***Nat Genet*** **49, 946–952 (2017).**

18. Diness, J. G. ***et al.*** **The KCa2 Channel Inhibitor AP30663 Selectively Increases Atrial Refractoriness, Converts Vernakalant-Resistant Atrial Fibrillation and Prevents Its Reinduction in Conscious Pigs.** ***Front Pharmacol*** **11, 159 (2020).**

19. Adelman, J. P. SK channels and calmodulin. ***Channels*** **10, 1–6 (2015).**

20. Lee, C.-H. & MacKinnon, R. Activation mechanism of a human SK-calmodulin channel complex elucidated by cryo-EM structures. ***Science*** **360, 508–513 (2018).**

21. Brown, B. M., Shim, H., Christophersen, P. & Wulff, H. Pharmacology of Small- and Intermediate-Conductance Calcium-Activated Potassium Channels. ***Annu Rev Pharmacol*** **60, 219–240 (2019).**

22. Zhang, X.-D. ***et al.*** **Coupling of SK channels, L-type Ca2+ channels, and ryanodine receptors in cardiomyocytes.** ***Sci Rep-uk*** **8, 4670 (2018).**

23. Hirschberg, B., Maylie, J., Adelman, J. P. & Marrion, N. V. Gating of recombinant small-conductance Ca-activated K+ channels by calcium. ***The Journal of general physiology*** **111, 565 581 (1998).**

24. Xia, X.-M. ***et al.*** **Mechanism of calcium gating in small-conductance calcium-activated potassium channels.** ***Nature*** **395, 503–507 (1998).**

25. Saucerman, J. J. & Bers, D. M. Calmodulin mediates differential sensitivity of CaMKII and calcineurin to local Ca2+ in cardiac myocytes. ***Biophys J*** **95, 4597 4612 (2008).**

26. Kincaid, R. L. & Vaughan, M. Direct comparison of Ca2+ requirements for calmodulin interaction with and activation of protein phosphatase. ***Proc National Acad Sci*** **83, 1193–1197 (1986).**

27. Bergeron, Z. L. & Bingham, J.-P. Scorpion toxins specific for potassium (K+) channels: a historical overview of peptide bioengineering. ***Toxins*** **4, 1082–119 (2012).**

28. Lamy, C. ***et al.*** **Allosteric Block of KCa2 Channels by Apamin.** ***J Biol Chem*** **285, 27067–27077 (2010).**

29. Weatherall, K. L., Seutin, V., Liégeois, J.-F. & Marrion, N. V. Crucial role of a shared extracellular loop in apamin sensitivity and maintenance of pore shape of small-conductance calcium-activated potassium (SK) channels. ***Proc National Acad Sci*** **108, 18494–18499 (2011).**

30. Nolting, A., Ferraro, T., D'hoedt, D. & Stocker, M. An Amino Acid Outside the Pore Region Influences Apamin Sensitivity in Small Conductance Ca2+-activated K+ Channels. ***J Biol Chem*** **282, 3478–3486 (2007).**

31. Grunnet, M. ***et al.*** **Pharmacological modulation of SK3 channels.** ***Neuropharmacology*** **40, 879–887 (2001).**

32. Simó-Vicens, R. ***et al.*** **A new negative allosteric modulator, AP14145, for the study of small conductance calcium-activated potassium (KCa2) channels.** ***Brit J Pharmacol*** **174, 4396–4408 (2017).**

33. Diness, J. G. ***et al.*** **Termination of Vernakalant-Resistant Atrial Fibrillation by Inhibition of Small-Conductance Ca2+-Activated K+ Channels in Pigs.** ***Circulation Arrhythmia Electrophysiol*** **10, e005125 (2017).**

34. Jenkins, D. P. ***et al.*** **Negative Gating Modulation by (R)-N-(Benzimidazol-2-yl)-1,2,3,4-tetrahydro-1-naphthylamine (NS8593) Depends on Residues in the Inner Pore Vestibule: Pharmacological Evidence of Deep-Pore Gating of KCa2 Channels.** ***Mol Pharmacol*** **79, 899–909 (2011).**

35. Strøbæk, D. ***et al.*** **Inhibitory Gating Modulation of Small Conductance Ca 2+ -Activated K + Channels by the Synthetic Compound (R) -N -(Benzimidazol-2-yl)-1,2,3,4-tetrahydro-1-naphtylamine (NS8593) Reduces Afterhyperpolarizing Current in Hippocampal CA1 Neurons.** ***Mol Pharmacol*** **70, 1771–1782 (2006).**

36. Jenkins, D. P. ***et al.*** **NS8593-Mediated Negative Gating Modulation Depends on Residues in the Inner Pore Vestibule of Kca2 Channels.** ***Biophys J*** **98, 125a (2010).**

37. Haugaard, M. M. ***et al.*** **Pharmacologic inhibition of small-conductance calcium-activated potassium (SK) channels by NS8593 reveals atrial antiarrhythmic potential in horses.** ***Heart Rhythm*** **12, 825–835 (2015).**

38. Sørensen, U. S. ***et al.*** **Synthesis and Structure−Activity Relationship Studies of 2-(N-Substituted)-aminobenzimidazoles as Potent Negative Gating Modulators of Small Conductance Ca2+-Activated K+ Channels.** ***J Med Chem*** **51, 7625–7634 (2008).**

39. Hirschberg, B., Maylie, J., Adelman, J. P. & Marrion, N. V. Gating properties of single SK channels in hippocampal CA1 pyramidal neurons. ***Biophys J*** **77, 1905 1913 (1999).**

40. Lu, L. ***et al.*** **Molecular Coupling of a Ca2+-Activated K+ Channel to L-Type Ca2+ Channels via α-Actinin2.** ***Circ Res*** **100, 112–120 (2007).**

41. Ishii, T. M., Maylie, J. & Adelman, J. P. Determinants of Apamin and d -Tubocurarine Block in SK Potassium Channels. ***J Biol Chem*** **272, 23195–23200 (1997).**

42. Shamsaldeen, Y. A. ***et al.*** **Role of SK channel activation in determining the action potential configuration in freshly isolated human atrial myocytes from the SKArF study.** ***Biochem Bioph Res Co*** **512, 684–690 (2019).**

43. Maylie, J., Bond, C. T., Herson, P. S., Lee, W. & Adelman, J. P. Small conductance Ca2+-activated K+ channels and calmodulin. ***J Physiology*** **554, 255–261 (2004).**

44. McManus, O. B., Blatz, A. L. & Magleby, K. L. Sampling, log binning, fitting, and plotting durations of open and shut intervals from single channels and the effects of noise. ***Pflügers Archiv - European J Physiology*** **410, 530–553 (1987).**

45. Landowne, D., Yuan, B. & Magleby, K. L. Exponential Sum-Fitting of Dwell-Time Distributions without Specifying Starting Parameters. ***Biophys J*** **104, 2383–2391 (2013).**

46. Magleby, K. L. & Pallotta, B. S. Burst kinetics of single calcium-activated potassium channels in cultured rat muscle. ***J Physiology*** **344, 605–623 (1983).**

47. Colquhoun, D. & Sakmann, B. Fast events in single-channel currents activated by acetylcholine and its analogues at the frog muscle end-plate. ***J Physiology*** **369, 501–557 (1985).**

48. Sine, S. M. & Steinbach, J. H. Activation of acetylcholine receptors on clonal mammalian BC3H-1 cells by low concentrations of agonist. ***J Physiology*** **373, 129–162 (1986).**

49. Habermann, E. & Reiz, K. G. [On the biochemistry of bee venom peptides, melittin and apamin]. ***Biochem Z*** **343, 192–203 (1965).**

50. Rohaim, A. ***et al.*** **Open and Closed Structures of a Barium-Blocked Potassium Channel.** ***J Mol Biol*** **432, 4783–4798 (2020).**

51. Quayle, J. M., Standen, N. B. & Stanfield, P. R. The voltage-dependent block of ATP-sensitive potassium channels of frog skeletal muscle by caesium and barium ions. ***J Physiology*** **405, 677–697 (1988).**

52. Park, J. B., Kim, H. J., Ryu, P. D. & Moczydlowski, E. Effect of Phosphatidylserine on Unitary Conductance and Ba2+ Block of the BK Ca2+–activated K+ Channel. ***J Gen Physiology*** **121, 375–398 (2003).**

53. Bello, R. A. & Magleby, K. L. Time-irreversible Subconductance Gating Associated with Ba2+ Block of Large Conductance Ca2+-activated K+ Channels. ***J Gen Physiology*** **111, 343–362 (1998).**

54. Neyton, J. & Miller, C. Discrete Ba2+ block as a probe of ion occupancy and pore structure in the high-conductance Ca2+ -activated K+ channel. ***J Gen Physiology*** **92, 569–586 (1988).**

55. Vergara, C., Alvarez, O. & Latorre, R. Localization of the K+ Lock-in and the Ba2+ Binding Sites in a Voltage-Gated Calcium-Modulated Channel. ***J Gen Physiology*** **114, 365–376 (1999).**

56. Hurst, R. S., Latorre, R., Toro, L. & Stefani, E. External barium block of Shaker potassium channels: evidence for two binding sites. ***J Gen Physiology*** **106, 1069–1087 (1995).**

57. Wulff, H., Gutman, G. A., Cahalan, M. D. & Chandy, K. G. Delineation of the Clotrimazole/TRAM-34 Binding Site on the Intermediate Conductance Calcium-activated Potassium Channel, IKCa1*. ***J Biol Chem*** **276, 32040–32045 (2001).**

58. Nguyen, H. M. ***et al.*** **Structural Insights into the Atomistic Mechanisms of Action of Small Molecule Inhibitors Targeting the KCa3.1 Channel Pore.** ***Mol Pharmacol*** **91, mol.116.108068 (2017).**

Table 1: Full recording inventory (* p< 0.05, ** p < 0.01, *** p < 0.001)

	Control	Apamin	AP14145
Complete dataset characteristics			
Number of recordings	16	11	9
Total duration of recordings (s)	746	1577	1033
Total number closing events	10915	8032	5534
Total number of bursts	2282	1690	723
Burst duration (ms)	328 ± 136	259 ± 149	570 ± 184
Single channel patches			
Number of recordings	5	4	6
Total duration of recordings (s)	372	1125	737
Mean P_o	0.32 ± 0.16	0.10 ± 0.03	0.21 ± 0.12
Burst frequency (bursts.s^{-1})	3.56 ± 1.10	0.57 ± 0.30 *	1.06 ± 0.36 *
Very long closed event analyses			
Number of recordings	4	4	3
Total duration of recordings (s)	367	1125	720
Mean P_o	0.28 ± 0.21	0.10 ± 0.04	0.03 ± 0.01
Number of bursts	386 ± 192	91 ± 33	189 ± 76
Burst frequency (bursts.s^{-1})	3.97 ± 1.31	0.57 ± 0.30	0.99 ± 0.48
Total number of closed events > 1s	15	90	76
Total number of closed events > 2.9s	0	42	26
Frequency of closed events > 1s (events.10s^{-1})	0.22 ± 0.16	1.36 ± 0.35 *	1.27 ± 0.52
Frequency of closed events > 2.9s (events.10s^{-1})	0.00 ± 0.00	0.63 ± 0.15 **	0.38 ± 0.06 ***
% time in closed events > 1s	3.4 ± 2.3	78.7 ± 10.5 ***	63.6 ± 18.1 **
% time in closed events > 2.9s	0 ± 0	66 ± 16 **	49 ± 23 *
P_o excluding closed events > 1s	0.28 ± 0.21	0.43 ± 0.19	0.19 ± 0.13
P_o excluding closed events > 2.9s	0.28 ± 0.21	0.29 ± 0.17	0.16 ± 0.11
P_o preceding closed events > 1s	0.05 ± 0.02	0.16 ± 0.07	0.12 ± 0.10
P_o preceding closed events > 2.9s	NA	0.11 ± 0.07	0.11 ± 0.09
P_o after closed events > 1s	0.06 ± 0.04	0.13 ± 0.05	0.11 ± 0.07
P_o after closed events > 2.9s	NA	0.15 ± 0.09	0.11 ± 0.07
Intra-burst analyses			
Number of recordings	16	11	9
Total duration of recordings (s)	300	452	313
A_{low} (pA)	0.54 ± 0.03	0.54 ± 0.05	0.38 ± 0.03
Weight A_{low}	0.49	0.61	0.80
A_{high} (pA)	0.76 ± 0.03	0.74 ± 0.04	0.58 ± 0.06
Weight A_{high}	0.51	0.39	0.20
$Tau_{o,s}$ (ms)	4.01 ± 0.11	3.61 ± 1.00	4.59 ± 0.76
Weight $Tau_{o,s}$	0.62	0.65	0.42
$Tau_{o,l}$ (ms)	34.8 ± 9.3	20.9 ± 3.6	36.6 ± 11.5
Weight $Tau_{o,l}$	0.38	0.35	0.58
$Tau_{c,s}$ (ms)	1.59 ± 0.19	0.75 ± 0.10	3.50 ± 0.81
Weight $Tau_{c,s}$	0.56	0.64	0.63
$Tau_{c,i}$ (ms)	13.5 ± 1.2	5.1 ± 0.5	32.0 ± 6.8
Weight $Tau_{c,i}$	0.44	0.36	0.37
Inter-burst analyses			
Number of recordings	4	4	3
Total duration of recordings (s)	367	1125	720
Total number closing events	7212	3116	3422
$Tau_{c,l}$ (ms)	132 ± 19	153 ± 129	233 ± 38
Weight $Tau_{c,l}$	1.0	0.42	0.78
$Tau_{c,vl}$ (ms)	NA	11752 ± 7131	10265 ± 7249
Weight $Tau_{c,vl}$	NA	0.58	0.22

Table 2: Flickery activity analyses (*** p < 0.001)

		Time in Flickery activity (s, %)		
Group	**Non-VL time (s)**	**10 sequential events (C < 5 ms, O < 1 ms)**	**20 sequential events (C < 5 ms, O < 1 ms)**	**40 sequential events (C < 10 ms, O < 1 ms)**
Control	241.6	0.46 s, 0.19%	0 s, 0%	0 s, 0%
Apamin	82.2	11.89 s, 14.47% ***	2.60 s, 3.16% ***	4.26 s, 5.19% ***
AP14145	183.3	0.06 s, 0.03%	0 s, 0%	0 s, 0%

Figure legends

Figure 1*: rSK2 exhibits two opening amplitudes. Raw traces in A and B show single SK channel openings as downward deflections from baseline (dashed grey line).* ***A****. At -50 mV holding potential, the majority of rSK2 channels show two clear unitary amplitudes (A_{low} and A_{high}).* ***B****. Non-contiguous sweeps showing a number of clear transitions from A_{low} to A_{high} (↓), and vice versa (↑).* ***C.*** *Representative amplitude histogram (left) and exponential distribution of open dwell-time histogram (right) constructed from all opening events for a single patch. These distributions (dashed lines) clearly show two distinguishable amplitude components, and two distinguishable open durations (solid lines).* ***D.*** *Summary data for opening amplitudes across all control patches (n=16). All 16 patches exhibited A_{high}, whereas slightly fewer (12 of 16) patches also exhibited a significant A_{low} component as determined by maximum likelihood fitting (left panel). The two amplitudes are separated by approximately 50% of the mean A_{low}, suggesting a sub-conductance conformation (right panel).* ***E****. We next separated the tail regions (shaded areas) of the amplitude distributions into A_{high} events (top panels) and A_{low} events (bottom panels) to assess whether the two amplitude classes exhibited any differences in open duration. Representative histograms show that the mean open durations of the two amplitude classes are not different.* ***F****. While relatively few (n = 6) patches had sufficient opening events to be decomposed in this way, summary analyses of those 6 patches also suggest that there was no difference in either the short ($\tau_{o,s}$) or long ($\tau_{o,l}$) open dwell-times between the two amplitude classes.* ***G****. Further supporting this assertion, there is no correlation ($r^2 = 0.006$) between amplitude and open duration for all events in a single patch, although the independent high and low amplitudes can still be clearly visualized as horizontally oriented clusters around the mean of each amplitude level. Error bars in panels* ***D*** *and* ***F*** *represent mean and SEM, respectively. *** $p < 0.001$ vs. A_{low}.*

Figure 2: *Summary of control rSK2 single channel kinetics.* ***A****. As indicated by representative data in figure 1, most rSK2 channels exhibit open dwell-time distributions best fit by 2 exponentials ($\tau_{o,s}$, and $\tau_{o,l}$).* Dashed distribution represents overall fit, with individual components in solid lines. ***B***. *When assessing all (n = 16) control patches, only 2 patches exhibited maximum likelihood fit for 1 rather than 2 open duration components.* ***C.*** *On average, $\tau_{o,s}$, and $\tau_{o,l}$ were separated by approximately an order of magnitude in control patches, although both distributions were relatively broad. As mentioned in the methods section, because these recordings were analyzed by a different technician, the absolute values of the two open durations $\tau_{o,s}$ = 4.0 ± 0.1 ms, and $\tau_{o,l}$ = 34.8 ms are slightly longer than we have previously published.*[23] ***D****. A representative closed duration distribution (dashed line) indicating the three typical rSK2 closed dwell-times in solid lines (short: $\tau_{c,s}$, intermediate: $\tau_{c,i}$, and long: $\tau_{c,l}$), and the control burst delimiter*, *as previously.*[23] ***E****. All control patches (n=16) permitted fitting of the short ($\tau_{c,s}$) and intermediate ($\tau_{c,i}$) closed durations, however only patches with one identifiable channel and at least 10-s continuous recording were subjected to*

*burst analysis for distinguishing the long ($\tau_{c,l}$) and very long ($\tau_{c,vl}$) closed durations (see Methods). **F**. The three closed dwell-time components in these control patches were again separated by approximately 2 orders of magnitude (from several ms to several hundred ms). Bold horizontal bars and error bars in panels **C** and **F** represent mean and SEM, respectively.*

***Figure 3:** AP14145 reduces unitary currents and modestly slows open channel kinetics, whereas open channel dynamics are unaffected by apamin. **A**. Representative amplitude distributions for apamin (top) and AP14145 (bottom), showing left-shifted and narrower amplitude profiles for AP14145. **B.** Representative open duration distributions for apamin (top) and AP14145 (bottom), neither of which were altered compared to control. Dashed lines in A and B represent overall distribution, with individual components as solid lines. **C**. AP14145 decreased the number of patches with a distinguishable high amplitude class of channel openings - only 4 of 9 AP14145 patches exhibited A_{high} (right panel). **D**. AP14145 also decreased the mean amplitude of the A_{low} opening events to 71% of control A_{low}. **E**. AP14145 modestly reduced the fraction of patches (6/9) that exhibited a distinguishable short open duration ($\tau_{o,s}$), relative to control. **F**. Neither apamin nor AP14145 impacted the mean duration of either short or long classes of channel opening ($\tau_{o,s}$ or $\tau_{o,l}$) compared to control. Bold horizontal bars and error bars in panels **D** and **F** represent mean and SEM, respectively. *** $p < 0.001$ vs. control; † $p < 0.05$ vs. control.*

***Figure 4:** Apamin abbreviates and AP14145 prolongs short and intermediate channel closures during burst periods. Raw traces in A show SK channel openings as downward deflections from baseline (dashed grey line). **A.** Representative raw traces for burst behavior in control, apamin, and AP14145 recordings. **B**. Representative closed duration distribution showing the intra-burst components (solid line), and overall distribution (dashed line) for apamin and AP14145. **C**. The great majority of patches for both apamin (n = 11) and AP14145 (n = 9) exhibited two distinguishable intra-burst closed durations. **D**. The mean durations for both $\tau_{c,s}$ and $\tau_{c,i}$ were markedly altered by both apamin and AP14145. apamin shortened both components ($\tau_{c,s}$ = 47%, $\tau_{c,i}$ = 37%, both relative to control), whereas AP14145 prolonged both components ($\tau_{c,s}$ = 221%, $\tau_{c,i}$ = 237%, again both relative to control). Bold horizontal bars and error bars in panel **D** represent mean and SEM, respectively. † $p < 0.05$ vs. control; ** $p < 0.01$ vs. control; # $p < 0.001$ vs. apamin.*

***Figure 5:** Both apamin and AP14145 introduce a fourth closed duration that represents very long periods of channel inactivity. **A**. Diary plots of channel P_o averaged over epochs of 500 ms duration. Mean P_o indicated for each condition is the average of all epochs in the recording. When channel activity is visualized over a time scale of 10s of seconds, it is clear that both apamin and AP14145 introduce long periods of inactivity that are not present in control recordings, and not observable on the scale of 100's of milliseconds. **B**. Representative closed duration distribution showing the inter-burst components (solid line), and overall distribution (dashed line) for apamin and AP14145. In addition to the long closed duration ($\tau_{c,l}$) present in control*

patches, inter-burst histograms for both apamin and AP14145 exhibit an additional (fourth) very long closed ($\tau_{c,vl}$) component in the presence of apamin or AP14145. ***C****. In contrast to the control recordings, all single-channel patches treated with apamin (n = 4) and AP14145 (n = 3) exhibited the new fourth duration.* ***D****. The mean long closed duration, $\tau_{c,l}$, was unaffected by apamin and AP14145, and neither ($\tau_{c,l}$ or $\tau_{c,vl}$) differed between apamin and AP14145. Bold horizontal bars and error bars in panel* ***D*** *represent mean and SEM, respectively.* **†** *$p < 0.05$ vs. control.*